Materials and Manufacturing Processes, 25: 658–664, 2010

ISSN: 1042-6914 print/1532-2475 online
DOI: 10.1080/10426910903496888

Taylor & Francis
Taylor & Francis Group

Investigation of Antiadhesive Coatings for Nanoimprinting Lithography

Z. W. Zhong[1], X. C. Shan[2], and Y. C. Yao[1]

[1]*School of Mechanical and Aerospace Engineering, Nanyang Technological University, Singapore, Singapore*
[2]*Singapore Institute of Manufacturing Technology, Singapore, Singapore*

This article presents an investigation of antiadhesive coatings for nanoimprinting lithography. To get the optimum parameters of the coating process, a surface-contact angle goniometer and an atomic force microscope were used for detailed comparison of the coated surfaces produced with different process parameters. With the antiadhesive coating, the contact angle of deionized water on the mold surfaces changed from 30°–90°. The relationships between the coated surface characteristics and the coating parameters were experimentally studied. Under certain conditions, before it reached ~90° the contact angle increased significantly with increased coating time, baking time and solution concentration. The nanoimprinting process was then performed using the mold coated with selected parameters, and the imprinting results showed that the coating was effective to reduce the interfacial forces between the mold and the polymer for nanoimprinting. The contact angle measurements and the atomic force microscope investigation showed that the antiadhesive layer had no obvious degradation after the imprinting process.

Keywords Antiadhesive coating; Contact angle; Micro- and nanoscale patterns; Nanoimprinting lithography.

Introduction

Advanced technologies have been developed for various applications on micro- and nanoscales such as microlenses [1], microactuators [2], microsensors [3, 4], micromachining [5], microassemblies [6, 7], and microsystems [8]. The continuous development of lower cost, higher throughput, and higher resolution lithography brings new challenges to the microelectronics industry [9–12]. Great industrial efforts have been made for the next-generation lithography techniques such as electron beam lithography [13, 14], X-ray lithography [15], etc.

The commercialization of microelectromechanical systems (MEMS) demands the extension of existing processes and new process developments [16–18]. Current microfabrication processes of MEMS include the LIGA process [19], bulk micromachining [20], free-form microfabrication [21], surface micromachining [22]. Despite the important role of Si in MEMS fabrication, there is increasing interest in metallic and polymeric microstructures [23] with high aspect ratios for applications such as magnetic microsystems and microfluidic devices [24]. Thick photoresists, such as polymethylmethacrylate and SU-8, are widely used in the fabrication of such microstructures in MEMS [25, 26].

Nanoimprinting [27, 28] is a powerful tool for large-area replication of nanometer-scale features [29]. It has also been explored in recent years to fabricate carbon nanotube arrays [30]. There are also electric imprint lithography [31] and direct metal nanoimprinting (embossing) [32]. Ultraviolet (UV) nanoimprinting, as a derivative of nanoimprinting, uses a UV-curable resin [33] and UV illumination to cure the resin during processing [34–38]. During a nanoimprinting process, the stamp undergoes significant deformation in patterned zones, and the deformation strongly depends on the stamp material, array size, and stamp thickness [39]. A fast nanoimprinting lithography process is proposed based on the use of stamps with an integrated heater [40]. A silicon/SU8 hybrid-material stamp has been developed to combine nanometer and micrometer structures [41].

A key issue of nanoimprinting lithography is the sticking between the resist and the stamp mold. The high-density nanoscale features of the mold increase the surface area contacting the polymer [42]. This leads to adhesion between the mold and polymer, which can be so strong that the imprinted layer may be torn away from the substrate during demolding [43]. Therefore, a nonsticking interface between the polymer and the stamp is needed for clean demolding [42]. Teflon-like antiadhesion layers can be used to lower the surface energy of the stamp to help demolding [43]. Self-assembled monolayers such as octadecyltrichlorosilane (OTS) [44], polybenzoxazine [45], and fluorodecyl-trichlorosilane (FDTS) [46] can also be adopted as an antiadhesive layer to increase the lifetime of the stamp mold [44].

This paper presents an investigation of antiadhesive coatings for nanoimprinting lithography. Experiments were conducted to demonstrate the capability of the imprinting process for reproducing micro- and nano-scale patterns. To get the optimum parameters of the coating process, a surface-contact angle goniometer, and an atomic force

Received October 22, 2009; Accepted November 9, 2009
Address correspondence to Z. W. Zhong, School of Mechanical and Aerospace Engineering, Nanyang Technological University, 50 Nanyang Avenue, Singapore 639798, Republic of Singapore; Fax: (65) 6791 1859; E-mail: mzwzhong@ntu.edu.sg

microscope were used for detailed comparison of the coated surfaces produced with different process parameters. The relationships between the coated surface characteristics (the contact angle of deionized water, etc.) and the coating parameters (the coating time, baking time and solution concentration, etc.) were experimentally investigated. Then, the nanoimprinting process was performed using the mold coated with the selected parameters.

The nanoimprinting lithography studied

A semiautomated hot embossing system was used in this study. Eight-inch Si wafers were used as the substrate, which were cleaned with 40% nitric acid, deionized water, isopropanol, and O_2-plasma etching before resist-coating. NEB-22, a high resolution negative resist, was spin-coated as the resist polymer. The layer thickness was ~250 nm.

After resist-coating, the wafer was baked for 30 sec at 100°C. A spectroscopic ellipsometer was used to measure the thickness of the spin-coated polymer film at different points. The thickness uniformity was ±0.28%, which is well acceptable for nanoimprinting.

An 8-inch Si mold was used with patterns of dots and lines. The polymer layer was brought into contact with the mold in a vacuum chamber. The mold and the wafer were heated in the vacuum chamber to the desired process temperature (130°C) that was above the resist's glass transition temperature (80°C). Then the system applied a press force (30 kN) between the mold and the resist layer. This force was held constantly for 10 min to force the polymer into the mold completely. After the mold and the polymer were cooled down to ~50°C, the process force was released. The wafer was then separated from the mold with the reversed microstructures replicated onto the resist. This process generated nanoscale lines and pillars before reactive ion etching (RIE). It is demonstrated that the imprinting lithography has the potential to replicate micro and nanolevel patterns in a large area up to an 8-inch wafer.

Optical microscopy was used to characterize the patterns in different fields of the wafer, and this revealed that the printing process was uniform. The imprinting uniformity in smaller patterns was also studied by measuring the same patterns at the four edges and the center of the wafer. The measurement results are summarized in Table 1. They reveal that the uniformity of line depth is ±1.7%, and that of line width is 0.25% for the grating patterns. Imprinting lithography can be very uniform over a significantly large area. The width and the depth of the grating patterns in the selected areas are almost identical.

As process repeatability and mold durability are two key issues in making imprinting lithography a manufacturing technology, the same mold was used to imprint NEB-22 over 5 times, and the mold and the NEB-22 profile were examined every time. No noticeable changes were found in the NEB-22 profile or the mold.

However, after imprinting, the mold surface could be contaminated by residual polymer. When this happened, it was impossible to make a subsequent imprint without time-consuming cleaning. The contamination resulted from the adhesion between the mold and the polymer. To obtain good repeatability and mold durability, it is necessary to provide a nonsticking interface between the mold and the polymer. Therefore, a simple method of antiadhesive coating for nanoimprinting lithography was investigated, and this is presented in Sections 3 and 4.

Table 1.—The line width and depth of imprinted patterns.

Location	Depth (nm)	Line width (nm)
A	437.5	210.0
B	436.9	212.5
C	438.0	208.8
D	436.9	209.4
E	437.3	212.3

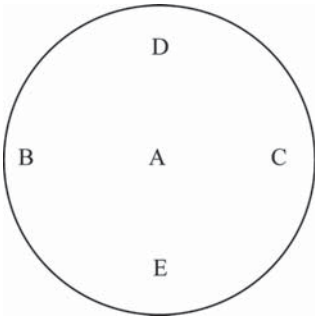

Contact angles of antiadhesive coatings

Surfactant molecules such as FDTS can be deposited on the mold surface, either as a liquid phase or as a vapor phase [46]. In this study, FDTS antiadhesive coatings deposited as a liquid phase were investigated. The anti-adhesive layer can reduce the surface energy. This ability can be quantified by the value of the contact angle of the coating. A higher contact angle means lower surface energy. Based on the contact angles, good surface coating parameters can be found.

A surface-contact-angle goniometer was used to measure the surface contact angles of deionized water on the coatings. To explore the relationships between the surface contact angle and the antiadhesive coating parameters, different concentration FDTS solutions, 2.5 mM (millimole/L), 5 mM, 10 mM, 15 mM, and 20 mM, were prepared, and Si wafers were coated with the FDTS solutions.

First, two pieces of clean silicon wafers were prepared, and the bare wafers' contact angles were measured. Then, the two wafers were coated with 10 mM FDTS solution using different methods. Spin-coating was performed on the first wafer with a recipe of 3000 rpm and 20 seconds. Immersion coating was conducted on the other wafer, which was immersed into the solution for 10 min followed by rinsing with fresh heptan solvent for 2 min. After coating, the wafers were dried using nitrogen gas, and their contact angles were then measured at four different locations on each wafer for 5 times at each location. Figure 1 shows the average measurement results.

The results in Fig. 1 show that the FDTS spin and immersion coatings can obviously lead to increased surface contact angles of the wafers, but the immersion coating is better compared with spin-coating. The reason is that it

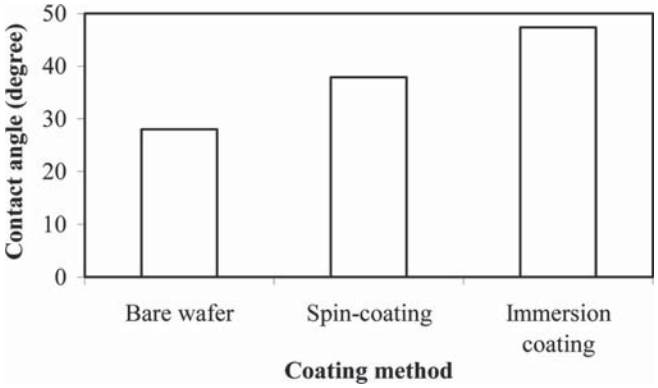

FIGURE 1.—Average contact angle of the wafers without and with the coating.

needs sufficient time to form the anti-adhesive FDTS layer in the coating processes. During the 20 seconds of spin-coating, the reaction for condensation of FDTS on the Si surface cannot finish. However, in the immersion coating process, the reaction time is sufficient, which means the coating time is an important parameter for this antiadhesive coating process.

Effect of Coating Time

To investigate the effect of coating time, 9 wafers were immersed into the 10 mM FDTS solution for 1, 4, 7, 10, 13, 16, 20, 30, and 50 min, respectively, followed by rinsing with fresh heptan solvent for 2 min. After rinsing, the wafers were dried using nitrogen gas. Then their contact angles at four different locations on each wafer were measured for 5 times at each location. Figure 2 shows the average measurement results. The coating time has an obvious effect on the immersion coating process. When the coating time prolonged from 1–20 min, the contact angle increased significantly from 35.4°–91.5°. After that, the contact angle kept constant when the coating time changed from 20 min to 30 min or 50 min.

The results show that after the wafer is dipped into the FDTS solution, a period of time is needed to form the antiadhesive layer on the wafer surface. For the 10 mM

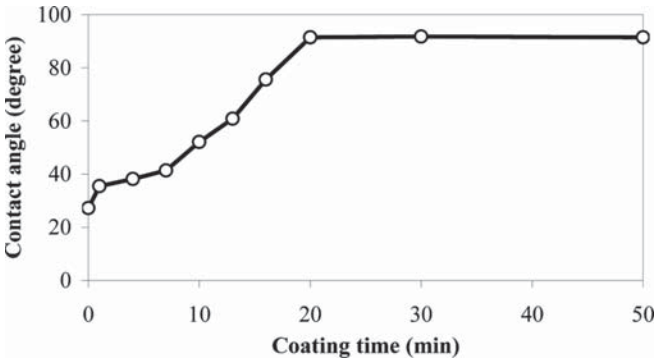

FIGURE 2.—Average contact angle versus coating time (10 mM FDTS solution).

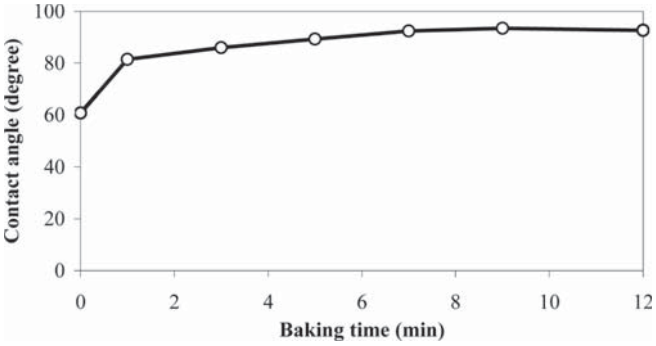

FIGURE 3.—Average contact angle versus baking time (wafers were coated for 13 min in 10 mM FDTS solution).

solution, the reaction time is about 20 min. The surface contact angle changes from about 30° to over 90°, which is well accepted for imprinting. After 20 min, the coating process keeps equilibrium, and the surface contact angle of the coating cannot increase anymore.

Effect of Baking

Baking time is another interesting parameter in the coating process. Six wafers were immersion-coated for 13 min in 10 mM FDTS solution, followed by rinsing with fresh heptan solvent for 2 min. The wafers were then dried using nitrogen gas. After that, the 6 wafers were baked at 100°C for 1, 3, 5, 7, 9, and 12 min, respectively. Then their contact angles at four different locations on each wafer were measured for 5 times at each location to investigate the effect of baking time.

Figure 3 shows the average measurement results. The surface contact angle increases from 60.8° to 93.5°, when the baking time increases from 0–9 min. There is no significant change of the contact angles when the baking time is longer than 7 min. After coating, baking at a high temperature can remove the moisture in the coating layer and increase the contact angle of the coating layer. On the other hand, baking can also improve the adhesion of the coating layer, so that the coating layer can be more reliable in the imprinting process. The results show that 7–9 min

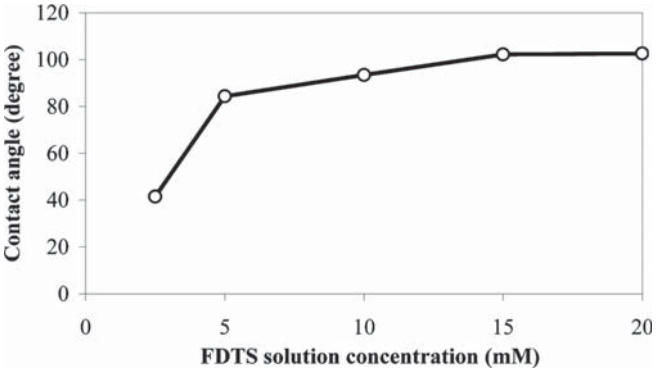

FIGURE 4.—Average contact angle versus FDTS solution concentration (wafers were coated for 13 min and baked at 100°C for 9 min).

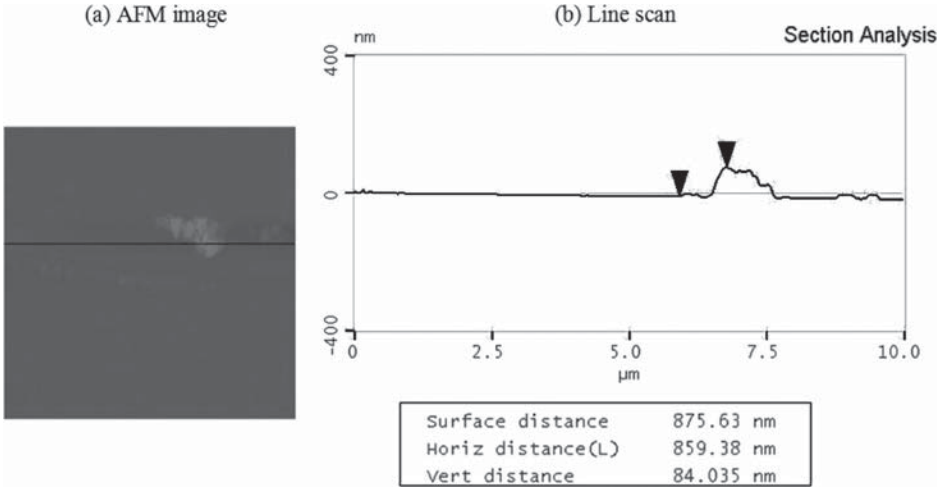

FIGURE 5.—Surface topography of the 10 mM FDTS coating (coating time = 4 min) without baking (contact angle = 38.2°).

baking at 100°C is needed for obtaining the antiadhesive coating.

Effect of Solution Concentration

FDTS solutions with concentration of 2.5 mM, 5 mM, 10 mM, 15 mM, and 20 mM were prepared. Clean wafers were immersed into these solutions for 13 min followed by rinsing with fresh heptan solvent for 2 min. The wafers were dried using nitrogen gas and baked for 9 min at 100°C. Then their contact angles at four different locations on each wafer were measured for 5 times at each location to investigate the effect of solution concentration. Figure 4 shows the average measurement results.

The results in Fig. 4 show that under the same processing conditions (13 min coating and 9 min baking), the contact angle would increase when solution concentration changed from 2.5–15 mM. But the contact angle had no significant changes with 15 mM and 20 mM solutions. The reaction rate varies with changing in solution concentration. The reaction is slower in a diluted solution compared with that in a thick one. That is the reason for the small surface contact angle of the wafer coated with the 2.5 mM concentration. To obtain the same surface contact angle, coatings in different concentration solutions require different coating times. A diluted solution requires a longer coating time.

SURFACE TOPOGRAPHY OF FDTS COATINGS

Atomic force microscopes (AFMs) have many applications in microelectronics and MEMS [47, 48]. In this work, an AFM was used to measure the surface topography of the wafers with FDTS coatings to investigate the relationships between the surface roughness and the coating parameters, as well as the relationship between the surface contact angle and the surface roughness.

Coating Time Effect

Figures 5 and 6 show examples of AFM images of the wafers coated with different coating times. The images show

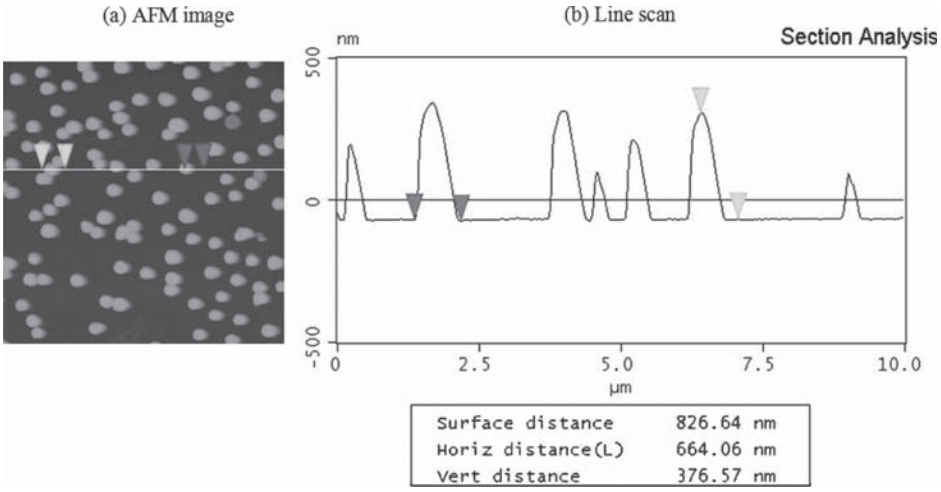

FIGURE 6.—Surface topography of the 10 mM FDTS coating (coating time = 13 min) without baking (contact angle = 60.8°).

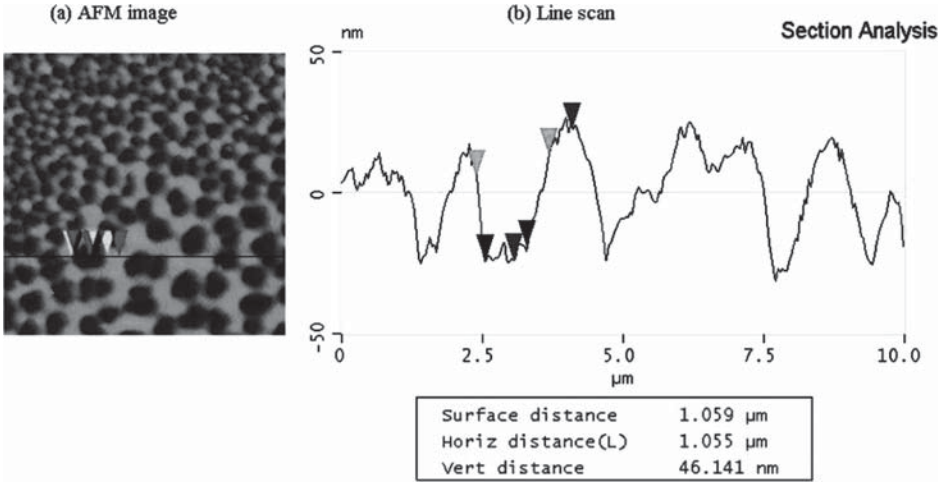

FIGURE 7.—AFM image of the coating obtained using a 10 mM FDTS solution with a coating time of 4 min and baking at 100°C for 9 min (contact angle = 68°).

that the surface roughness of the coatings increases with coating time. This may be due to the bulk polymerization of the precursor molecules. There may also be particles deposited on the surfaces, and the particle number and size increase when the coating time prolongs from 4–13 min. As discussed in the "Effect of Coating Time" section, the surface contact angle of the coatings also increases, when the coating time is increased.

Other AFM images also indicate the same trend. For example, when wafers were coated with a 2.5 mM FDTS solution, both the coating surface roughness and the surface contact angle increased with the coating time prolonged from 13–40 min.

As the antiadhesive coating is concerned, a bigger surface contact angle and lower surface roughness are preferred. However, these two aspects are conflicting with each other in the coating process. There has to be a trade-off between the surface contact angle and the surface roughness.

Solution Concentration

The AFM images of wafers with surface contact angles of about 90° coated using different concentration solutions were also obtained. When the contact angle was about 90°, there was no regular relationship between the surface roughness and the solution concentration. The particle number and size of the coatings were also similar to each other. However, to obtain surface contact angles of about 90°, different solution concentrations require different coating times: a lower concentration requires a longer coating time.

Obtaining Smooth Coating Surfaces

As discussed in the "Coating Time Effect" section, after the FDTS coating process, the surface roughness and the surface contact angle will increase. For nanoimprinting processes, an antiadhesion coating with a large contact angle

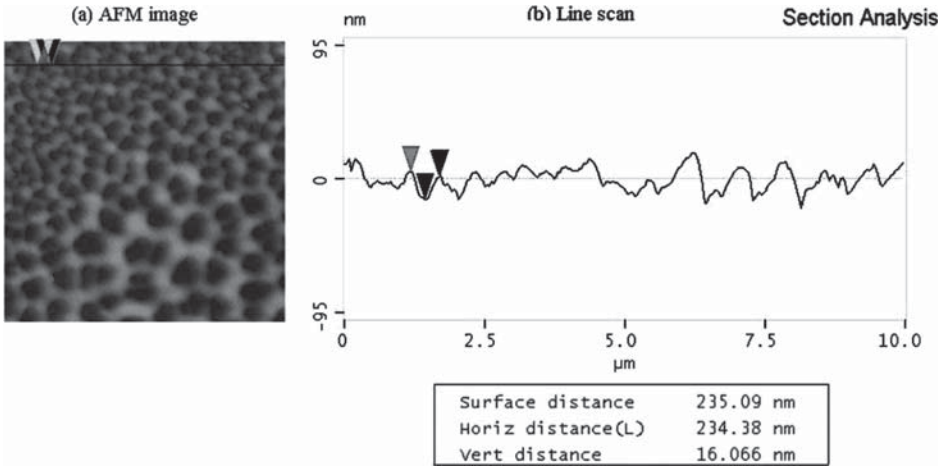

FIGURE 8.—AFM image of the mold surface after the imprinting process.

value and a small roughness value is desired. However, these two aspects conflict in the coating process. A trade-off between the surface contact angle and the surface roughness of the coating is inevitable.

On the other hand, it can be assumed that there might be undissolved particles in the solution, which also contributed to rough coating surfaces. Therefore, filters were used to remove the undissolved particles from the solution in the following coating process: Immersion coating was performed using a 10 mM FDTS solution with a coating time of 4 min and baking at 100°C for 9 min. To reduce the size of particles, 0.2 μm filters were used to remove the undissolved particles before coating. Figure 7 shows the AFM image of the coating obtained. It can be seen that after filtering the FDTS solution and using a shorter coating time (4 min), the coating surface is relatively smooth and uniform. On the other hand, the surface contact angle is 68°, which is acceptable considering that there has to be a trade-off between the surface roughness and the surface contact angle.

Effect of the Antiadhesion Coating

To evaluate the effect of the FDTS coating, test imprints were conducted. The mold with various microstructures was coated with the 10 mM filtered FDTS solution. The recipe was 4 min coating followed by baking at 100°C for 9 min. Optical micrographs of the imprinted substrate with different patterns revealed that no resist lift-off could be observed in these areas, meaning a clean demolding process was performed in imprinting.

To examine the durability of the anti-adhesive ability of the FDTS coating, the contact angles of the mold surface were measured before and after the imprinting process, and they were 97.8° and 97.5°, respectively. This confirmed that there was no noticeable change in surface contact angles before and after imprinting.

The AFM was used to investigate the mold surface after the imprinting process. It can be seen from Fig. 8 that after one cycle of the imprinting process, the FDTS layer became more uniform. This means that the coating layer did not degrade after the imprinting process. A uniform and smooth coating layer is essential for the nanoimprinting process.

Conclusions

Antiadhesive coatings were investigated for the nanoimprinting lithography. With the coating, the contact angle of the mold surface increased from 30° to 90°. On the other hand, its surface roughness also increased after coating. Under certain conditions, before it reached ~90°, the contact angle increased significantly with increased coating time, baking time, and solution concentration. The nanoimprinting process was performed using the mold coated with selected parameters, and the imprinting results showed that the FDTS coating was effective to reduce the interfacial forces between the mold and the polymer for nanoimprinting. In addition, the contact angle measurement and the AFM investigation showed that the FDTS antiadhesive layer had no significant degradation after the imprinting process.

References

1. Hocheng, H.; Wen, T.T.; Yang, S.Y. Replication of microlens arrays by gas-assisted hot embossing. Materials and Manufacturing Processes **2008**, *23*, 261–268.
2. Sun, J.; Zhong, Z.W. Finite element analysis of a IBM suspension integrated with a PZT microactuator. Sensors and Actuators A-Physical **2002**, *100*, 257–263.
3. Hautefeuille, M.; O'Flynn, B.; Peters, F.; O'Mahony, C. Miniaturised multi-MEMS sensor development. Microelectronics Reliability **2009**, *49*, 621–626.
4. Ghisi, A.; Fachin, F.; Mariani, S.; Zerbini, S. Multi-scale analysis of polysilicon MEMS sensors subject to accidental drops: Effect of packaging. Microelectronics Reliability **2009**, *49*, 340–349.
5. Ali, M.Y.; Mohammad, A.S. Effect of conventional edm parameters on the micromachined surface roughness and fabrication of a hot embossing master microtool. Materials and Manufacturing Processes **2009**, *24*, 454–458.
6. Zhong, Z.W.; Yeong, C.K. Development of a gripper using SMA wire. Sensors and Actuators A-Physical **2006**, *126* (2), 375–381.
7. Shuang, B.; Chen, J.; Li, Z. Microrobot based micro-assembly sequence planning with hybrid ant colony algorithm. International Journal of Advanced Manufacturing Technology **2008**, *38* (11–12), 1227–1235.
8. Wang, J.C.; Hsieh, M.Z. Applying the one-column, many pencil local scanning maskless lithography technology to micro-RP system. International Journal of Advanced Manufacturing Technology **2009**, *41* (7–8), 727–733.
9. Zhong, Z.W. Wire bonding using insulated wire and new challenges in wire bonding. Microelectronics International **2008**, *25* (2), 9–14.
10. Moore, G.E. Lithography and the future of Moore's law, Proc. SPIE-Int Soc. Opt. Eng., 1995. pp. 2–17.
11. Okazaki, S. Lithography for ULSI, Proc. SPIE-Int Soc. Opt. Eng., 1995. pp. 18–32.
12. Zhong, Z.W. Fine and ultra-fine pitch wire bonding: challenges and solutions. Microelectronics International **2009**, *26* (2), 10–18.
13. Kim, H.S.; Ahn, S.; Kim, D.W.; Oh, T.S.; Ahn, S.J. Efficient electron beam condensing for low-energy microcolumn lithography. Microelectronics Journal **2008**, *39* (1), 94–98.
14. Lv, S.L.; Song, Z.T.; Feng, S.L. Fabrication of arrays of line with nanoscale width and large length by electron beam lithography with high-precision stage. Microelectronics Journal **2008**, *39* (9), 1126–1129.
15. Chou, M.C.; Pan, C.T.; Wu, T.T.; Wu, C.T. Study of deep X-ray lithography behaviour for microstructures. Sensors and Actuators, A: Physical **2008**, *141* (2), 703–711.
16. Madou, M.J. *Fundamentals of Microfabrication: the Science of Miniaturization*; CRC Press: Boca Raton, FL, 2002.
17. Zhong, Z.W.; Lim, S.C.; Asundi, A. Effects of thermally induced optical fiber shifts in V-groove arrays for optical MEMS. Microelectronics Journal **2005**, *36* (2), 109–113.
18. Jasinski, P. Micro solid oxide fuel cells and their fabrication methods. Microelectronics International **2008**, *25* (2), 42–48.
19. Wang, Q.; Duan, Y.; Ding, Y.; Lu, B.; Xiang, J.; Yang, L. Investigation on LIGA-like process based on multilevel imprint lithography. Microelectronics Journal **2009**, *40* (1), 149–155.
20. Tao, Y.; Esashi, M. Macroporous silicon-based deep anisotropic etching. Journal of Micromechanics and Microengineering **2005**, *15* (4), 764–770.

21. Wu, D.; Fang, N.; Sun, C.; Zhang, X. Stiction problems in releasing of 3D microstructures and its solution. Sensors and Actuators, A: Physical **2006**, *128* (1), 109–115.
22. Varadan, V.K.; Jiang, X.; Varadan, V.V. *Microstereolithography and other Fabrication Techniques for 3D MEMS*; John Wiley & Sons: New York, 2001.
23. Zhong, Z.W.; Wang, Z.F.; Tan, Y.H. Chemical mechanical polishing of polymeric materials for MEMS applications. Microelectronics Journal **2006**, *37* (4), 295–301.
24. Triltsch, U.; Feldmann, M.; Boese, C.; BuÌˆttgenbach, S. Simulation tool for proximity effects in high aspect ratio UV-lithographic patterning. Sensors and Actuators, A: Physical **2008**, *142* (1), 429–433.
25. Yang, R.; Soper, S.A.; Wang, W. A new UV lithography photoresist based on composite of EPON resins 165 and 154 for fabrication of high-aspect-ratio microstructures. Sensors and Actuators, A: Physical **2007**, *135* (2), 625–636.
26. Zhong, Z.W.; Wang, Z.F.; Zirajutheen, B.M.P.; Tan, Y.S.; Tan, Y.H. Polishing of poly(methyl methacrylate), polycarbonate, and SU-8 polymers. Materials Science-Poland **2007**, *25* (1), 103–112.
27. Lee, J.H.; Yang, K.y.; Hong, S.H.; Lee, H.; Choi, K.W. Fabrication of 70 nm narrow metal nanowire structure on flexible PET film by nanoimprint lithography. Microelectron Eng **2008**, *85* (4), 710–713.
28. Wu, C.C.; Hsu, S.L.C.; Liao, W.C. A photo-polymerization resist for UV nanoimprint lithography. Microelectron Eng **2009**, *86* (3), 325–329.
29. Tallal, J.; Peyrade, D.; Lazzarino, F.; Berton, K.; Perret, C.; Gordon, M.; Gourgon, C.; Schiavone, P. Replication of sub-40 nm gap nanoelectrodes over an 8-in. substrate by nanoimprint lithography. Microelectron Eng **2005**, *78–79* (1–4), 676–681.
30. Yin, L.; Liu, H.; Ding, Y.; Lan, H.; Lu, B. Fabrication of carbon nanotube arrays for field emission and sensor devices by nanoimprint lithography. Microelectronics Journal **2009**, *40* (3), 604–607.
31. Ahn, Y.S.; Chen, Y.; Thomas Hahn, H. A resist for electric imprint lithography. Microelectron Eng **2009**, *86* (3), 392–396.
32. Buzzi, S.; Robin, F.; Callegari, V.; Löffler, J.F. Metal direct nanoimprinting for photonics. Microelectron Eng **2008**, *85* (2), 419–424.
33. Pietarinen, J.; Kalima, V.; Pakkanen, T.T.; Kuittinen, M. Improvement of UV-moulding accuracy by heat and solvent assisted process. Microelectron Eng. **2008**, *85* (2), 263–270.
34. Choi, J.H.; Jung, S.U.; Choi, D.G.; Jeong, J.H.; Lee, E.S. Direct soft UV-NIL with resist incorporating carbon nanotubes. Microelectron Eng. **2008**, *85* (1), 195–201.
35. Liu, H.; Jiang, W.; Ding, Y.; Tang, Y.; Lu, B.; Lan, H.; Shi, Y.; Yin, L. A novel loading and demoulding process control in UV nanoimprint lithography. Microelectron Eng. **2009**, *86* (1), 4–9.
36. Lee, J.; Park, S.; Choi, K.; Kim, G. Nano-scale patterning using the roll typed UV-nanoimprint lithography tool. Microelectron Eng. **2008**, *85* (5–6), 861–865.
37. Hong, S.H.; Hwang, J.Y.; Lee, H.; Lee, H.C.; Choi, K.W. UV nanoimprint using flexible polymer template and substrate. Microelectron Eng. **2009**, *86* (3), 295–298.
38. Jiang, W.; Ding, Y.; Liu, H.; Lu, B.; Shi, Y.; Shao, J.; Yin, L. Two-step curing method for demoulding in UV nanoimprint lithography. Microelectron Eng. **2008**, *85* (2), 458–464.
39. Merino, S.; Retolaza, A.; Juarros, A.; Schift, H. The influence of stamp deformation on residual layer homogeneity in thermal nanoimprint lithography. Microelectron Eng. **2008**, *85* (9), 1892–1896.
40. Tormen, M.; Malureanu, R.; Pedersen, R.H.; Lorenzen, L.; Rasmussen, K.H.; Lüscher, C.J.; Kristensen, A.; Hansen, O. Fast thermal nanoimprint lithography by a stamp with integrated heater. Microelectron Eng. **2008**, *85* (5–6), 1229–1232.
41. Carlberg, P.; Montelius, L.; Tegenfeldt, J. Nanoimprint in PDMS on glass with two-level hybrid stamp. Microelectron Eng. **2008**, *85* (1), 210–213.
42. Beck, M.; Graczyk, M.; Maximov, I.; Sarwe, E.L.; Ling, T.G.I.; Keil, M.; Montelius, L. Improving stamps for 10 nm level wafer scale nanoimprint lithography. Microelectron Eng **2002**, *61-62*, 441–448.
43. Tallal, J.; Gordon, M.; Berton, K.; Charley, A.L.; Peyrade, D. AFM characterization of anti-sticking layers used in nanoimprint. Microelectron Eng. **2006**, *83* (4-9 SPEC. ISS.), 851–854.
44. Wu, C.W.; Shen, Y.K.; Chuang, S.Y.; Wei, C.S. Anti-adhesive effects of diverse self-assembled monolayers in nanoimprint lithography. Sensors and Actuators, A: Physical **2007**, *139* (1-2 SPEC. ISS.), 145–151.
45. Chang, T.L.; Wang, J.C.; Chen, C.C.; Lee, Y.W.; Chou, T.H. A non-fluorine mold release agent for Ni stamp in nanoimprint process. Microelectron Eng **2008**, *85* (7), 1608–1612.
46. Bunker, B.C.; Carpick, R.W.; Assink, R.A.; Thomas, M.L.; Hankins, M.G.; Voigt, J.A.; Sipola, D.; De Boer, M.P.; Gulley, G.L. Impact of solution agglomeration on the deposition of self-assembled monolayers. Langmuir **2000**, *16* (20), 7742–7751.
47. Lu, Y.G.; Zhong, Z.W.; Yu, J.; Xie, H.M.; Ngoi, B.K.A.; Chai, G.B.; Asundi, A. Thermal deformation measurement of electronic packages using the atomic force microscope scanning moire technique. Rev Sci Instrum **2001**, *72* (4), 2180–2185.
48. Xie, H.M.; Asundi, A.; Boay, C.G.; Lu, Y.G.; Yu, J.; Zhong, Z.W.; Ngoi, B.K.A. High resolution AFM scanning Moire method and its application to the micro-deformation in the BGA electronic package. Microelectronics Reliability **2002**, *42* (8), 1219–1227.